Volume 22
Number 17
7 September 2020
Pages 5507-5846

Green Chemistry

Cutting-edge research for a greener sustainable future

rsc.li/greenchem

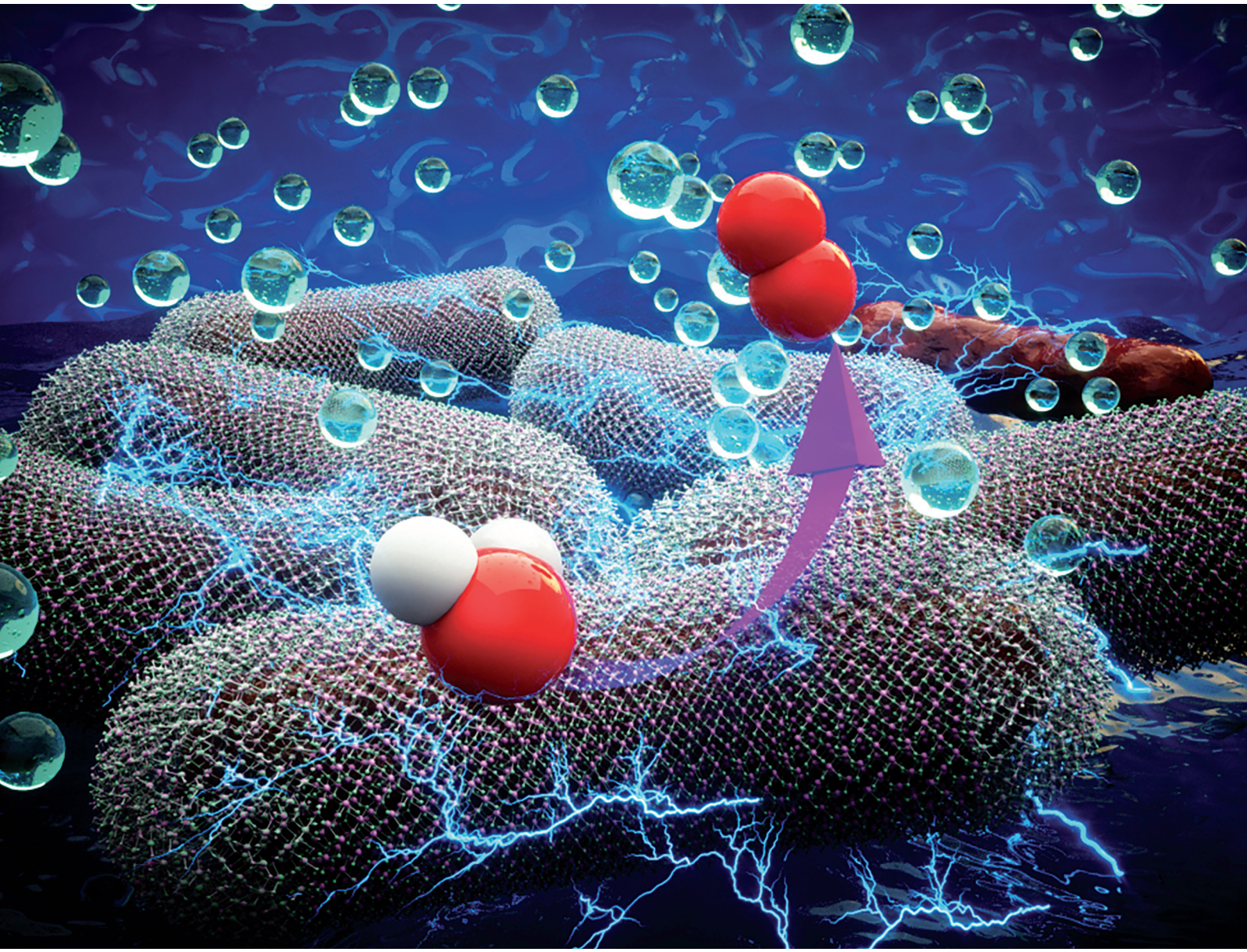

ISSN 1463-9262

ROYAL SOCIETY OF CHEMISTRY

PAPER

Pascal E. Saikaly *et al.*

Synthesis of an amorphous *Geobacter*-manganese oxide biohybrid as an efficient water oxidation catalyst

Green Chemistry

PAPER

View Article Online
View Journal | View Issue

Cite this: *Green Chem.*, 2020, **22**, 5610

Synthesis of an amorphous *Geobacter*-manganese oxide biohybrid as an efficient water oxidation catalyst†

Shafeer Kalathil, Krishna P. Katuri and Pascal E. Saikaly *

The development of a low cost and efficient oxygen evolution reaction (OER) catalyst has paramount importance to meet the future sustainable energy demand. Nature's photosynthetic machinery deploy manganese-based complex in the photosystem II to oxidize water. Inspired by nature, herein, we synthesized a high performing manganese-based OER catalyst using an electrochemically active and iron-rich bacterium, *Geobacter sulfurreducens*. The as-synthesized biohybrid catalyst (amorphous *Geobacter*-Mn_2O_3) produced a current density of 10 mA cm^{-2} at an overpotential of 290 ± 9 mV *versus* a reversible hydrogen electrode with a low Tafel slope of 59 mV dec^{-1}. The catalyst exhibited remarkable stability, evidenced through a long-term chronopotentiometry experiment. Multiple evidence showed that *G. sulfurreducens* contributed OER active elements (iron and phosphorus) to the biohybrid catalyst, and the as-synthesized *Geobacter*-Mn_2O_3 is amorphous. The amorphous structure of the biohybrid catalyst provided a large electrochemically active surface area and excess catalytic sites for the OER catalysis. In addition, Mn^{3+} present in the biohybrid catalyst is believed to be the precursor for oxygen evolution. The OER activity of the biohybrid catalyst outperformed commercial-Mn_2O_3, commercial-IrO_2 and most of the benchmark precious OER catalysts, thus supporting its suitability for large-scale applications. The proposed green approach to synthesize a biohybrid catalyst paves a new avenue to develop robust and cost-effective electrocatalysts for energy-related applications.

Received 20th December 2019,
Accepted 24th April 2020

DOI: 10.1039/c9gc04353e

rsc.li/greenchem

Introduction

There is an increasing global demand for energy, which is mainly supported by burning fossil fuels.[1,2] The current rate of consumption of fossil fuels, which are limited resources, may lead to their ultimate depletion and further increase in atmospheric carbon dioxide (CO_2) concentration, resulting in serious environmental pollution and climate change issues.[3] Hence, exploring alternative energy sources, in particular renewable energy sources, is highly warranted to protect our environment. Water is a unique source of energy since it serves as a cheap and abundant source of electrons.[4] Water oxidation or oxygen evolution reaction (OER) is a key process in solar fuel production, rechargeable metal–air batteries, and microbial electrosynthesis to produce either hydrogen or high-value chemicals/fuels from CO_2 reduction.[2–6] However, OER is kinetically sluggish and needs high energy input, which remain a bottleneck in water splitting.[5] Catalysts play a significant role in OER by lowering the overpotential required to oxidize water. To facilitate OER, great efforts have been made to develop efficient and affordable catalysts. Metal oxides of iridium and ruthenium are the most common electrocatalysts that are employed for OER.[7] However, their high cost, poor stability, and scarcity hinder the large-scale applications of these materials as OER catalysts.[7] Thus, there is an urgent need to develop earth-abundant, cost-effective, and efficient electrocatalysts for the facilitation of OER.

Manganese oxide (MnO_x)-based OER catalysts provide an alternative to the high-cost catalysts because of their earth abundance, non-toxicity, low cost and versatile redox properties.[4] Manganese (Mn) is a natural choice for OER as a Mn-based complex is the OER unit in the process of photosynthesis (PS II).[4,8] Thus, inspired by nature, numerous efforts have been made to develop Mn-based OER catalysts.[8] Mn occupies a unique position in catalysis because of its ability to exhibit different oxidation states and each state demonstrates distinct catalytic properties.[4,9] The Production of MnO_x heavily depends on chemical and physical methods used.[10,11] Chemical methods require rigorous reaction conditions such as high temperature and copious amount of toxic chemicals,

Division of Biological and Environmental Sciences & Engineering, Water Desalination and Reuse Center, King Abdullah University of Science and Technology, Thuwal 23955-6900, Saudi Arabia. E-mail: pascal.saikaly@kaust.edu.sa

†Electronic supplementary information (ESI) available. See DOI: 10.1039/c9gc04353e

while physical methods consume high energy to produce MnO_x.

Here, we propose a microbial method using the bacterium *Geobacter sulfurreducens* to synthesize an amorphous *Geobacter*-Mn_2O_3 biohybrid as an efficient OER catalyst. *G. sulfurreducens* is a naturally abundant dissimilatory metal reducing bacterium and has the highest electricity producing capacity in microbial electrochemical systems.[12–15] It shows a great respiratory versatility using a variety of soluble (*e.g.*, fumarate) and insoluble (*e.g.*, metal oxides) terminal electron acceptors.[15] *G. sulfurreducens* communicates with solid electron acceptors such as electrodes, by discharging the metabolically generated electrons through a unique respiratory pathway called extracellular electron transfer (EET).[12,13] EET in *G. sulfurreducens* involves outer-membrane c-type cytochromes (OM c-Cyts) and nanowires/pili (extension of c-Cyts) as electron conduits to transport the electrons from the cell interior to the external environment.[14,15] c-Cyts in *G. sulfurreducens* are rich in iron (Fe) due to the presence of heme groups, which are the key components in the EET. The hallmark of *G. sulfurreducens* is their ability to uptake Fe to maintain intracellular Fe concentration using a homodimeric protein, ferric uptake regulator (Fur).[16] Isotopic experiments showed a threefold higher Fe concentration in *G. sulfurreducens* as compared to *Escherichia coli*, suggesting the Fe richness in the cells.[17] It is known that Fe-based electrocatalysts usually show the highest OER activity[18] and a recent study found that Fe is the actual OER site in Fe/Ni layered double hydroxides.[19] Moreover, *G. sulfurreducens* can act as a microbial factory to produce diverse nanomaterials and nanostructures. For example, *G. sulfurreducens* can produce noble metal nanoparticles (palladium, silver and gold), magnetite nanoparticles and reduced graphene oxide by employing the EET pathway.[5,20–23] Moreover, *G. sulfurreducens* plays a crucial role in the geo-biochemical cycling of Mn by reducing or oxidizing Mn compounds depending on their availability in nature and redox behavior.[24] The above-mentioned physiological advantages of *G. sulfurreducens* inspired us to choose *G. sulfurreducens* as an inoculum source for synthesizing an efficient *Geobacter*-Mn_2O_3 biohybrid electrocatalyst for the OER.

Experimental

Bacterial culture

G. sulfurreducens PCA (DSM 12127) was purchased from DSMZ-German Collection of Microorganisms and Cell Cultures. *G. sulfurreducens* was cultured in anaerobic serum bottles with 10 mM acetate as the electron donor and 50 mM fumarate as the electron acceptor in a defined medium (pH 7.0).[25] A gas purged (for 1 h with $N_2 : CO_2$—80 : 20%) anaerobic medium was transferred into the serum vials, followed by adjusting the solution pH under an N_2 environment in an anaerobic glove box (Labconco, USA). After media sterilization (121 °C, 20 min at 15 psi), the serum vials were inoculated with a *G. sulfurreducens* (3% v/v; $OD_{600\ nm}$) culture and incubated in a shaking incubator (Innova 40, New Brunswick Scientific, USA) for three days (200 rpm, 30 °C). Growth was monitored by measuring optical density ($OD_{600\ nm}$) using a UV-vis spectrometer (Varian Cary 50, Agilent Technologies).

Synthesis of amorphous *Geobacter*-Mn_2O_3

The as-grown 100 mL *G. sulfurreducens* solution ($OD_{600\ nm}$ = 0.6) was centrifuged (7000 rpm, 4 minutes) and the resulting red pellets (due to the presence of Fe containing c-Cyts on the cell membrane)[5] were washed with the defined medium (lacking fumarate), followed by re-suspending the pellet into the medium and centrifugation. The washed pellets were added to an anaerobic serum vial containing 100 mL of the anaerobic growth medium with acetate (20 mM, as the electron donor) and potassium permanganate ($KMnO_4$, 5 mM) as the sole electron acceptor. The serum bottles were incubated in a shaking incubator (200 rpm, 30 °C) for one day until the solution color changed from violet to dark brown, suggesting the reduction of Mn. The as-synthesized *Geobacter*-Mn_2O_3 was collected by centrifugation (10 000 rpm, 5 minutes). The collected material was washed six times with MilliQ water by gentle vortexing to remove any contribution of the media to the *Geobacter*-Mn_2O_3 biohybrid electrocatalyst. After washing, *Geobacter*-Mn_2O_3 was dried overnight (50 °C) and this dried sample was used for all the experiments. Several batches of experiments were conducted to reproduce the results. In addition, control tests using dead bacterial cells (heat-killed by autoclaving) and without the bacterial cells were conducted to evaluate the biological activity of *G. sulfurreducens* on $KMnO_4$ reduction.

Suppression of c-type cytochromes in *G. sulfurreducens*

The role of c-type cytochromes (c-Cyts) in the Mn reduction was deciphered by suppressing the formation of c-Cyts in *G. sulfurreducens*. The suppression of c-Cyts in *G. sulfurreducens* was performed as previously reported.[17] *G. sulfurreducens* was initially grown in an Fe-lacking defined medium. After three days of growth, the bacterium was re-inoculated in the defined medium (without Fe) with the addition of 30 μM bipyridine (an Fe chelator to suppress the production of OM c-Cyts) and grown for three days. The bipyridine treated cells were used as inoculum for the reduction of $KMnO_4$ by following the same procedure as mentioned above.

Characterization

Scanning transmission electron microscopy (STEM) analysis was performed on a FEI Titan 80–300 equipped with an energy dispersive X-ray (EDX) detector. For TEM analysis, samples were sonicated in ethanol solution for 30 minutes and a few drops of the sample were drop casted on a TEM Cu-grid. An electron energy loss spectrum (EELS) was obtained *via* scanning transmission electron microscopy-high angle annular dark-field (STEM-HAADF) mode with a probe size of ~1 nm. Scanning electron microscopy (SEM) analysis was performed on a TESCAN MIRA3 FEG-SEM equipped with the EDX detector, operating at 5 kV. An X-ray diffraction (XRD) analysis was

conducted on a Bruker D8 Advance X-ray diffractometer using Cu Kα irradiation. The survey and high-resolution X-ray photoelectron spectroscopy (XPS) spectra were obtained at fixed analyzer pass energies of 160 and 20 eV, respectively (model: ESCA 3400).

Inductively coupled plasma atomic emission microscopy (ICP-OES; Thermo Scientific) analysis was performed to estimate the elemental composition of samples. Bacterial cells were centrifuged, and the pellets were washed with MilliQ water six times to avoid any contribution from the media. The washed cells were soaked in nitric acid solution (70%) overnight and diluted to 5% prior to ICP-OES. The standard Fe solutions of 1 ppm and 10 ppm were used for the calibration. The wavelengths used were 238.20 nm, 239.56 nm and 259.94 nm, and the sample uptake used was 3 ml per minute. Triplicate measurements were conducted at each wavelength. UV-Vis spectra of $KMnO_4$ and *Geobacter*-Mn_2O_3 were recorded from 800–200 nm using a UV-Vis spectrometer (Varian Cary 50, Agilent Technologies).

Electrochemical experiments

The OER activity of amorphous *Geobacter*-Mn_2O_3 was measured by employing a rotating disc electrode (RDE). The catalyst for the OER was prepared as follows: the amorphous *Geobacter*-Mn_2O_3 (~2 mg) was dispersed in 500 μl of ethanol (96% v/v), 500 μl of deionized water and 15 μl of Nafion (as a binder). The solution was sonicated for 30 min. The obtained monodispersed solution (2 μl) was drop-casted onto a 3 mm glassy carbon disc electrode (loading concentration ~0.05 mg cm^{-2}) and was dried under a lamp for 1 h. The same protocol was followed to make a working electrode with commercial-Mn_2O_3 and commercial-IrO_2 (Sigma Aldrich). All the electrochemical analyses were performed in 1 M KOH (Sigma Aldrich, semiconductor grade, pellets, 99.99% trace metals basis) using a VMP3 potentiostat (BioLogic, France) at room temperature in a three-electrode system, where Pt coil and mercury/mercury oxide (Hg/HgO) were used as the counter and reference electrodes, respectively. Linear sweep voltammetry (LSV) experiments were conducted at a scan rate of 5 mV s^{-1} at a constant rotational speed of 1600 rpm. The durability of the biohybrid catalyst was investigated by running a long term chronopotentiometry measurement at a fixed current density of 10 mA cm^{-2} while recording the potential under a constant rotating speed of 1600 rpm. The electrochemically active surface area of the catalysts was determined by measuring double layer capacitance by performing cyclic voltammetry (CV) at various scan rates. All the measured potentials *vs.* the Hg/HgO were converted to RHE by the Nernst equation ($E_{RHE} = E_{Hg/HgO} + 0.0591\ pH + 0.140$). All the experiments were done at least in triplicates to reproduce the data.

Results and discussion

Fig. 1a shows a schematic of the synthesis of the *Geobacter*-Mn_2O_3 biohybrid by incubating *G. sulfurreducens* with MnO_4^- as the sole electron acceptor. *G. sulfurreducens* dissipates the respiratory electrons from the acetate oxidation to reduce MnO_4^- through the EET respiratory chain. The appearance of dark brown color (Fig. 1b) suggested the reduction of Mn took place. The EET pathway in *G. sulfurreducens* deploys a series of intra and extracellular conductive protein networks, which are aligned together from the cell-interior to cell-exterior.[13–15] Among the conductive protein networks, Fe (heme) rich OM c-Cyts play a key role in the final step of EET process.[13–15] The midpoint potential of the majority of OM c-Cyts involved in EET is in the range of −0.15 to −0.2 V *vs.* SHE,[26,27] while the

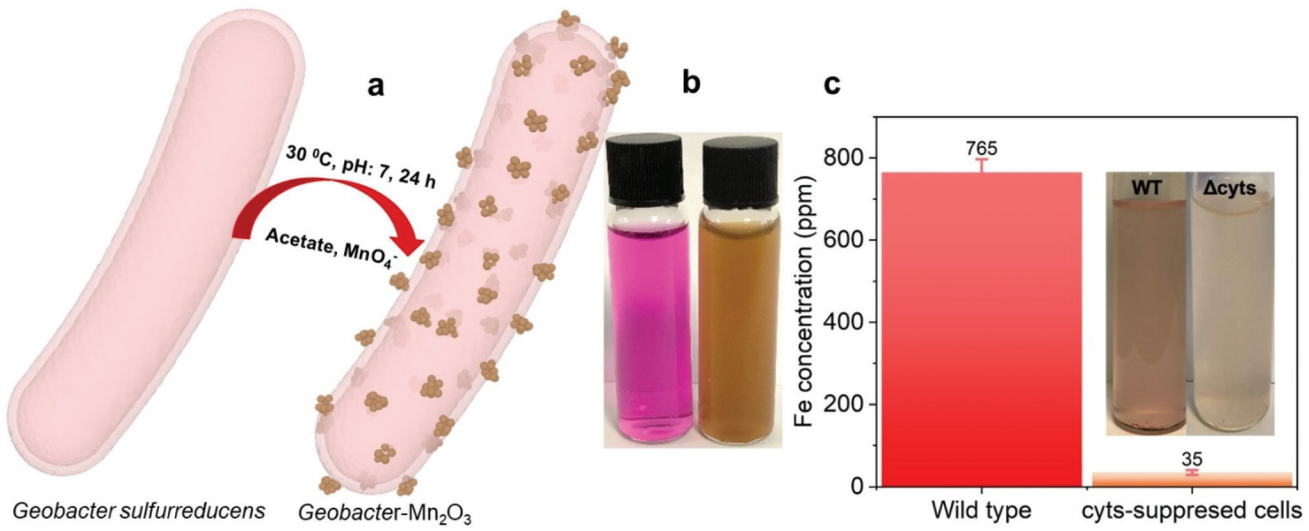

Fig. 1 (a) Schematic for the synthesis of amorphous *Geobacter*-Mn_2O_3 by *G. sulfurreducens*; (b) a digital photograph displaying the color change from violet ($KMnO_4$ precursor) to brown, suggesting the manganese reduction; and (c) Fe concentration data measured by ICP-OES for wild type (WT) and Cyts-suppressed cells (Δcyts), inset shows the fading of color for Δcyts cells compared to the WT because of low Fe content.

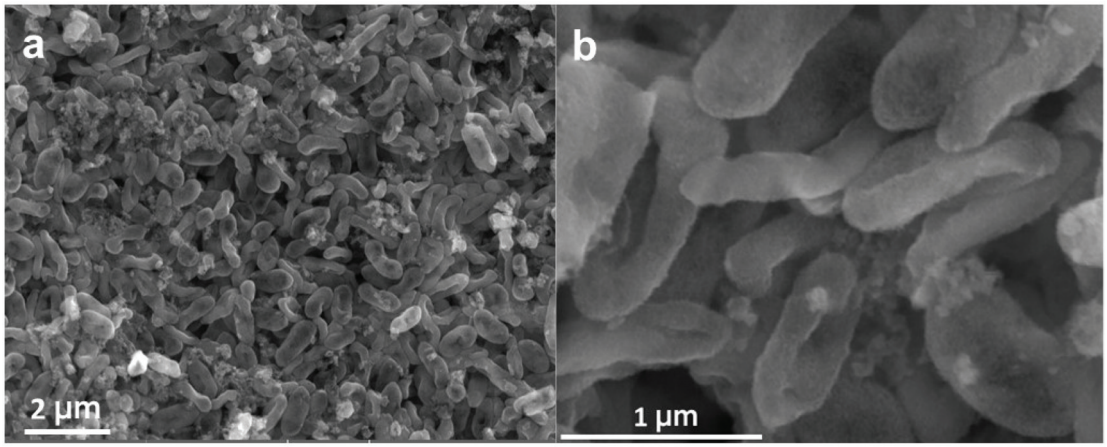

Fig. 2 Scanning electron microscopy (SEM) images of *G. sulfurreducens* cells decorated with Mn_2O_3 nanocrystals. (a) Low resolution, (b) high resolution SEM images.

reduction potential of MnO_4^- is 1.51 V *vs.* SHE. This huge difference in the potential gradient enables OM c-Cyts to reduce MnO_4^- relatively easily. To investigate the role of c-Cyts in the production of *Geobacter*-Mn_2O_3 biohybrid, we suppressed the production of c-Cyts in *G. sulfurreducens* by the addition of bipyridine. Bipyridine suppresses the production of c-Cyts in *G. sulfurreducens* by chelating with Fe at the growth stage.[17] The ICP-OES analysis showed a significant reduction in the Fe content of the suppressed (Δcyts) cells compared to the wild type (WT) cells (Fig. 1c). The reddish color substantially decreased in Δcyts cells (inset Fig. 1c) due to low Fe content. The Δcyts cells did not yield any Mn_2O_3 formation (Fig. S1†), suggesting that c-Cyts are essential to produce the *Geobacter*-Mn_2O_3 biohybrid. Further, there was no Mn reduction in the absence of live *G. sulfurreducens* cells or with heat-killed *G. sulfurreducens* cells. Taken together, these observations support that bacterial respiration by *G. sulfurreducens* was responsible for the production of *Geobacter*-Mn_2O_3 biohybrid.

An SEM analysis was performed to visualize the formation and morphology of the as-synthesized *Geobacter*-Mn_2O_3 biohybrid. The SEM image showed a uniform deposition of Mn_2O_3 nanocrystals on the surface of *G. sulfurreducens* cells (Fig. 2). The SEM-EDX spectrum (Fig. S2†) showed the elemental composition of *Geobacter*-Mn_2O_3 biohybrid as Mn (68 wt%), O (29.1 wt%), P (2.5 wt%) and Fe (0.4 wt%). P and Fe found in the hybrid originated from *G. sulfurreducens* cells.[5] STEM was used to investigate the chemical and structural nature of the as-synthesized *Geobacter*-Mn_2O_3 biohybrid. Fig. 3a shows the STEM-HAADF image of an individual *G. sulfurreducen* cell before incubation with MnO_4^- ions. The image depicts a typical morphology of the *G. sulfurreducens* cell, which is rod-shaped with a size of ~2 μM in length and ~0.5 μM in diameter.[5] After incubation with MnO_4^- ions, *Geobacter*-Mn_2O_3 biohybrid formed (Fig. 3b). Here, the micron-size bacterial cells served as a support for the decoration of Mn_2O_3 nanocrystals with uniform size and morphology on the surface of the cells. Elemental mapping demonstrated that *Geobacter*-Mn_2O_3 biohybrids were mainly made of Mn and oxygen (Fig. 3c and d). The high resolution TEM (HRTEM) image of *Geobacter*-Mn_2O_3 displayed no lattice fringes, suggesting the amorphous phase of the material (Fig. S3†), while the STEM image of commercial-Mn_2O_3 showed crystalline nature (Fig. S4†). The selected area electron diffraction (SAED) pattern of *Geobacter*-Mn_2O_3 exhibited halo diffraction rings, a characteristic observed for amorphous materials (Fig. 4a), while commercial-Mn_2O_3 showed well-defined sharp Braggs diffraction rings confirming its high crystallinity (Fig. 4b). An XRD analysis was performed to examine the crystal structure of *Geobacter*-Mn_2O_3 biohybrids and commercial-Mn_2O_3. The XRD profile of commercial-Mn_2O_3 showed sharp Bragg peaks, indicating high crystallinity, while *Geobacter*-Mn_2O_3 biohybrids showed broader peaks with poor resolution, a signature of the amorphous behavior (Fig. 4c). This observation is in well-agreement with the SAED results (Fig. 4a and b). The TEM-EDX spectroscopy analysis showed that in addition to Mn and oxygen, P and Fe were also present in the *Geobacter*-Mn_2O_3 biohybrid (Fig. S5†), which were derived from *G. sulfurreducens*, while Cu was derived from the TEM Cu-grid. The ICP-OES analysis further confirmed the presence of Fe (463 ± 21 ppm) in the amorphous *Geobacter*-Mn_2O_3 biohybrid.

EELS is a powerful tool to determine the oxidation state and bonding environment of metals in their oxide forms.[28–31] The EELS analysis shows the highest spatial and energy resolutions, which makes it suitable to characterize heterogeneous samples such as Mn and Fe oxides. Fig. 5a and b show oxygen K-edge and Mn-$L_{2,3}$ edge spectra of the amorphous *Geobacter*-Mn_2O_3 biohybrid and commercial-Mn_2O_3 captured on the nanointerface (see Fig. S4 and S6† for details). The spectra were recorded from 500 to 700 eV region using an energy dispersion of 0.1 eV. The EELS spectra of the *Geobacter*-Mn_2O_3 biohybrid and commercial-Mn_2O_3 showed similar patterns, suggesting that both have similar structures (Fig. 5a and b). The first peak ~529.2 eV in the O-K edge (O-K_a) represents the

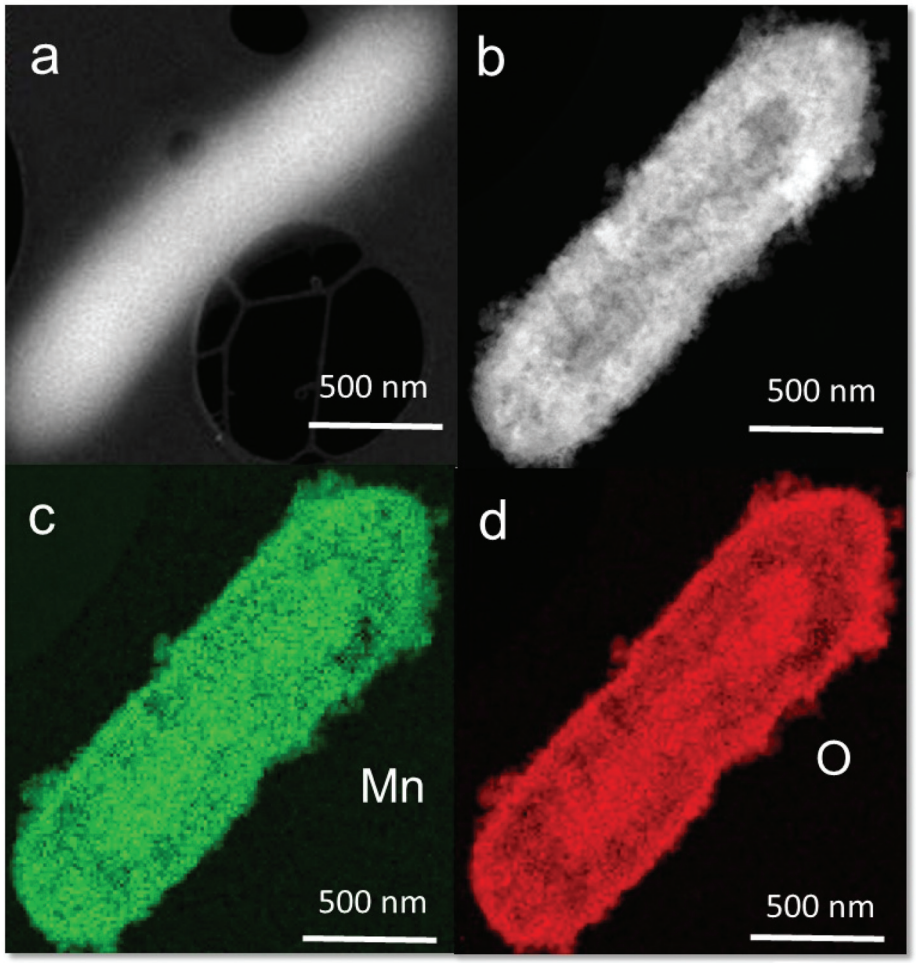

Fig. 3 Scanning transmission electron microscopy-high angle annular dark field (STEM-HAADF) images of a *G. sulfurreducens* cell before and after incubation with $KMnO_4$ (precursor). (a) *G. sulfurreducens* cell, (b) *Geobacter*-Mn_2O_3 biohybrid with *G. sulfurreducens* cell decorated with Mn_2O_3 nanocrystals. Elemental mapping of *Geobacter*-Mn_2O_3 showing (c) Mn and (d) oxygen.

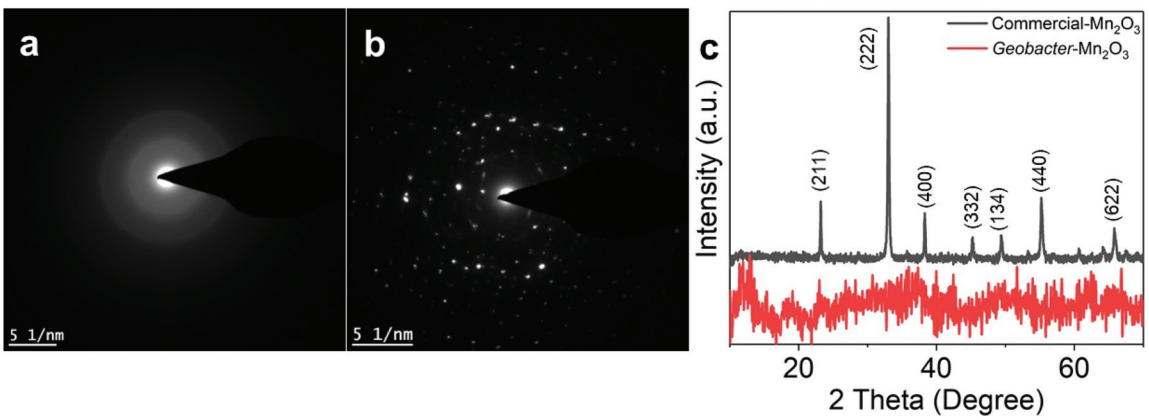

Fig. 4 Selected area diffraction (SAED) patterns of the (a) *Geobacter*-Mn_2O_3 biohybrid, (b) commercial-Mn_2O_3. (c) X-ray diffraction (XRD) patterns of *Geobacter*-Mn_2O_3 and commercial-Mn_2O_3.

electron transition from 1s core states to oxygen 2p states hybridized with Mn 3d orbitals.[28] The second peak ~540 eV (O-K_b) corresponds to probable unoccupied oxygen 2p states mixed with Mn 4sp states.[30] The energy separation between the first and second peaks is ~10.8 eV, which confirms the Mn_2O_3 phase in the biohybrid catalyst and the observation is consistent with earlier reports.[30,31] Mn-$L_{2,3}$ spectrum displays two white lines L_2 and L_3 because of the transition from $2p_{3/2}$

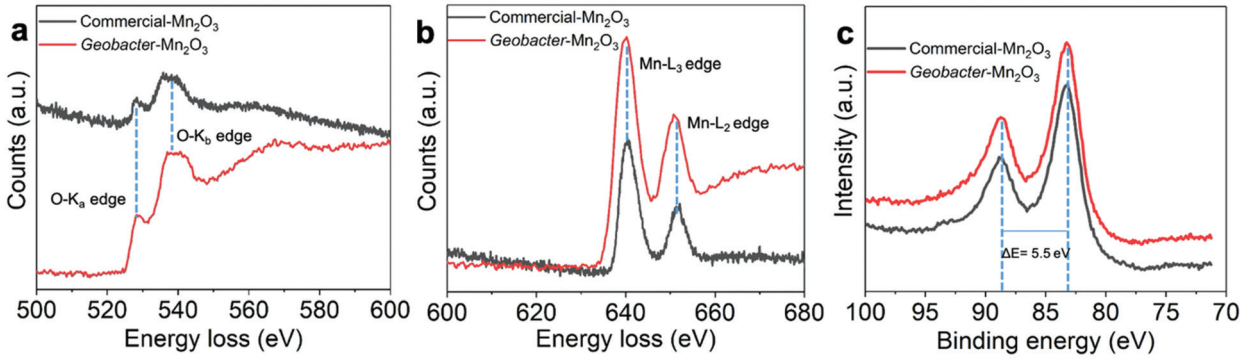

Fig. 5 (a) and (b) Electron energy loss spectra (EELS) recorded at the nanointerface of amorphous *Geobacter*-Mn_2O_3 and commercial-Mn_2O_3. The corresponding EELS images of the *Geobacter*-Mn_2O_3 and the location for the EELS spectra recorded are shown in Fig. S6.† (c) Mn 3s spectra of commercial-Mn_2O_3 and *Geobacter*-Mn_2O_3.

and $2p_{1/2}$ to 3d unoccupied states localized on the excited Mn ions.[28] The Mn valence state can be easily predicted by measuring the energy difference between M-L_3 and O-K_a (ΔE = M-L_3 − O-K_a).[28–31] The ΔE value measured for the amorphous *Geobacter*-Mn_2O_3 biohybrid is 111 eV, which was very close to a previously reported value for Mn_2O_3 (111.2 eV).[30] We further probed the oxidation state of Mn *via* XPS. The XPS spectra of commercial-Mn_2O_3 and *Geobacter*-Mn_2O_3 display similar profiles, indicating that they have similar structures (Fig. 5c and Fig. S7, S8†). The Mn 3s region in the XPS spectra can provide the oxidation state of Mn in its oxide form. Fig. 5c shows the Mn 3s peaks of commercial-Mn_2O_3 and *Geobacter*-Mn_2O_3 containing two, multiplet split components. The energy difference (ΔE) of the peak splitting for both the catalysts was determined to be 5.5 eV, which matches well with the Mn^{3+} oxidation state.[32] UV-Vis spectra can also provide some clues to understand the oxidation state of metal oxides. The *Geobacter*-Mn_2O_3 showed strong absorption in the visible region (300–600 nm) with a prominent peak at 430 nm (Fig. S9†). This peak arises from the d–d transitions of Mn^{3+} in the *Geobacter*-Mn_2O_3 as Mn^{3+} (d^4) forms a high spin complex.[33] Combined together, EELS, XPS and UV-Vis analyses support that the oxidation state of Mn in *Geobacter*-Mn_2O_3 is +3, and that the most probable chemical structure of the oxide in as-synthesized sample is Mn_2O_3.

The crystal structure of MnO_x and the oxidation states of Mn in the oxide form are crucial for the catalytic performance. Amorphous structures perform with higher OER activity over crystalline counterparts,[34] and the Mn^{3+} state triggers the OER more efficiently than the other oxidation states of Mn.[35] Most of the existing synthetic methods usually yield crystalline MnO_x where the oxidation state of Mn mainly stays in the +2 state.[34] Using our approach (*i.e.*, bacterial synthetic route), we were able to synthesize an amorphous structure of Mn oxide with Mn^{3+} state. In addition to acting as a reducing agent, *G. sulfurreducens* provided OER active elements (such as Fe and P) to the biohybrid catalyst (Fig. S2 and S5†) and acted as a micron size carbon support to the as-produced Mn_2O_3 nanocrystals (Fig. 3b). The carbon template provided by bacteria can render additional surface area, porosity and conductivity to the as synthesized biohybrid.

We employed the as-synthesized amorphous *Geobacter*-Mn_2O_3 biohybrid as an OER electrocatalyst and compared its performance with a commercial-Mn_2O_3 and commercial-IrO_2 catalyst. The OER activities of the catalysts were determined by conducting the LSV analysis at a scan rate of 5 mV s^{-1} under a constant rotating speed of 1600 rpm. A scan rate of 5 mV s^{-1} was chosen in the current study to compare the performance of our *Geobacter*-Mn_2O_3 biohybrid with previously reported OER electrocatalysts (Table 1 and Table S1†), which were also analyzed at a scan rate ≥5 mV s^{-1}. The overpotential for the OER is calculated by measuring the potential needed to generate a current density of 10 mA cm^{-2}, which is considered as a common practice in the literature.[36] The amorphous *Geobacter*-Mn_2O_3 biohybrid catalyst produced a geometrical

Table 1 OER activities of various Mn-based electrocatalysts

Catalyst	Overpotential (mV) @ 10 mA cm^{-2}	Tafel (mV dec^{-1})	Ref.
Amorphous *Geobacter*-Mn_2O_3	290	59	This study
Commercial-Mn_2O_3	370	80	This study
Amorphous manganese oxide	590	179	36
Mn oxide	540	n.a	43
Mn_2O_3	460	94	45
Calcined MnO_x on NCNT[a]	570	147	46
MnO_x/NCNT	410	91	47
Dandelion-like α-MnO_2	550	155	48
Fe doped-MnO_2	692	94	49
MnO_2	770	85	50
Mn_2O_3	410	99	51
Mn_3O_4	570	n.a	52
Mn-NG[b]	337	55	53
γ-MnO_2	427	n.a	54
Co- and Mn mixed oxides	450	35.8	55

[a] NCNT: nitrogen-functionalized carbon nanotube. [b] Mn-NG: mononuclear manganese embedded in nitrogen-doped graphene. n.a: not available in the literature.

current density of 10 mA cm^{-2} with an overpotential of 290 ± 9 mV (*vs.* RHE), while the commercial-Mn_2O_3 and commercial-IrO_2 displayed an overpotential of 370 ± 15 mV and 390 ± 18 mV (*vs.* RHE), respectively (Fig. 6a). Glassy carbon did not show any OER activity, as expected. A Tafel plot is useful to probe the kinetics and catalytic active sites of electrocatalysts.[5,36] The Tafel plot of amorphous *Geobacter*-Mn_2O_3 showed a lower slope value (59 mV dec^{-1}) than that of commercial-Mn_2O_3 (81 mV dec^{-1}) and commercial-IrO_2 (112 mV dec^{-1}), suggesting its superior OER activity (Fig. 6b). The chronopotentiometry experiment confirmed that the amorphous *Geobacter*-Mn_2O_3 biohybrid is highly stable for the OER even after 24 h of continuous measurements at a fixed current density of 10 mA cm^{-2} (Fig. 6c). TEM measurement after the stability test showed no significant changes in the structure of the catalyst, suggesting the structural robustness of the biohybrid catalyst (Fig. S10†). The absence of sharp diffraction peaks in the XRD pattern after chronopotentiometry further confirmed that the biohybrid kept its amorphous phase even after the long-term stability test (Fig. S11†).

The OER activity of the amorphous *Geobacter*-Mn_2O_3 biohybrid outperformed most of the Mn-based electrocatalysts (Table 1) and other benchmark OER catalysts including IrO_2 and RuO_2 (Table S1†). The OER activities of MnO_x largely depend on its chemical composition and crystallographic structure.[37] The amorphous structure of the *Geobacter*-Mn_2O_3 biohybrid offers a large surface area and high density of surface defects, which provide excess active sites for OER.[38] Previous studies have demonstrated that the amorphous phases of metal oxides outperform crystalline counterparts for the OER catalysis.[33] The X-ray absorption spectroscopy analysis of amorphous MnO_x has shown longer Mn–O distances due to Jahn–Teller-elongated Mn^{III}–O bonds.[38,39] This allows structural flexibility on the surface of MnO_x and enhances the OER activity. Electrochemically active surface area (ECSA) of the electrode is the actual surface area that is involved in a catalytic reaction.[40] ECSA is usually determined by measuring the double layer capacitance (C_{dl}) of the catalysts *via* performing CV at various scan rates.[40] The amorphous *Geobacter*-Mn_2O_3 biohybrid catalysts showed a C_{dl} of 26.8 mF cm^{-2}, which is

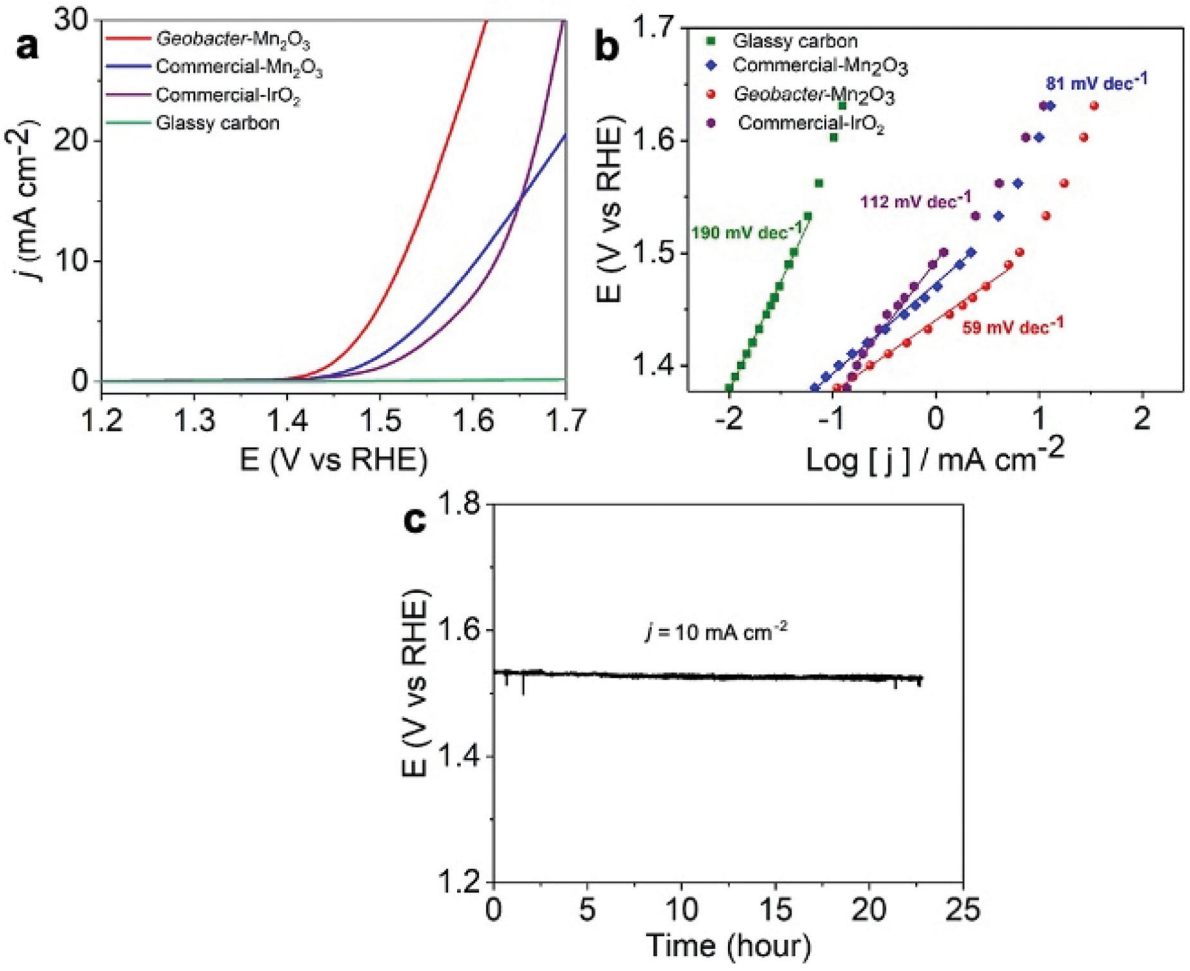

Fig. 6 (a) Linear sweep voltammetry (LSV) plots of amorphous *Geobacter*-Mn_2O_3, commercial-Mn_2O_3, commercial-IrO_2 and glassy carbon support at a scan rate of 5 mV s^{-1}; (b) Tafel plots of the used catalysts; and (c) stability test for the oxygen evolution reaction (OER) performance of amorphous *Geobacter*-Mn_2O_3 at a constant current density of 10 mA cm^{-2}. All experiments were conducted at a constant rotating speed of 1600 rpm.

nearly two times higher than that of the commercial-Mn_2O_3 (14 mF cm^{-2}) (Fig. S12†). The increased ECSA indicated highly porous nature of the *Geobacter*-Mn_2O_3 biohybrid, which provided excess catalytic sites for the OER. An *in situ* UV-vis spectroelectrochemical measurement revealed that Mn^{3+} serves as the precursor for the O_2 evolution.[41] Mn in the *Geobacter*-Mn_2O_3 biohybrid was present as Mn^{3+}, which can trigger O_2 evolution in the OER. In addition to its amorphous structure and the fact that Mn was present as Mn^{3+}, the superior OER activity of the *Geobacter*-Mn_2O_3 biohybrid could be due to the presence of Fe and P (Fig. S2 and S5†), which were provided by *G. sulffurreducens* cells during the MnO_4^- reduction process. Fe and P are known OER candidates that facilitate the catalytic activity.[42,43] A trace amount of Fe (ppm level) in the catalyst can drastically enhance the OER catalytic activity.[43] When pure *G. sulfurreducens* was used alone, no significant OER activity was observed (Fig. S13†). This was expected because one of the inherent problems of bacteria is that they possess low electrical conductivity,[44] which may suppress their catalytic activity.

Conclusions

In summary, we demonstrated a direct synthetic route to produce amorphous *Geobacter*-Mn_2O_3 biohybrid catalyst by *G. sulfurreducens* without the use of any toxic chemicals or high energy input. Further, we demonstrated that the as-produced amorphous *Geobacter*-Mn_2O_3 biohybrid is a promising OER electrocatalyst with an overpotential of 290 ± 9 mV *vs.* RHE to produce a current density of 10 mA cm^{-2} and a low Tafel slope of 59 mV dec^{-1}. The catalyst showed an excellent stability even after a long term chronoamperometry experiment. The OER activity of the biohybrid outperformed commercial-Mn_2O_3 and precious benchmark metal oxide electrocatalysts such as IrO_2 and RuO_2. The remarkable OER activity of the *Geobacter*-Mn_2O_3 biohybrid is attributed to the combination of its amorphous structure and the presence of additional OER active elements (Fe and P). The proposed cost-effective and green approach to synthesize Mn-based electrocatalysts at ambient experimental conditions using EET-capable bacteria opens the door for the synthesis of other high-performing and low-cost biohybrid electrocatalysts for various energy-related applications.

Conflicts of interest

There are no conflict of interests to declare.

Acknowledgements

This work was supported by Competitive Research Grant (URF/1/2985-01-01) from King Abdullah University of Science and Technology (KAUST).

References

1 A. Schoedel, Z. Ji and O. M. Yaghi, *Nat. Energy*, 2016, **1**, 16034.
2 K. P. Katuri, S. Kalathil, A. Ragab, B. Bian, M. F. Alqahtani, D. Pant and P. E. Saikaly, *Adv. Mater.*, 2018, **30**, 1707072.
3 M. F. Alqahtani, K. P. Katuri, S. Bajracharya, Y. Yu, Z. Lai and P. E. Saikaly, *Adv. Funct. Mater.*, 2018, **28**, 1804860.
4 M. M. Najafpour, G. Renger, M. Hołyńska, A. N. Moghaddam, E.-M. Aro, R. Carpentier, H. Nishihara, J. J. Eaton-Rye, J.-R. Shen and S. I. Allakhverdiev, *Chem. Rev.*, 2016, **116**, 2886.
5 S. Kalathil, K. P. Katuri, A. S. Alazmi, S. Pedireddy, N. Kornienko, P. M. F. J. Costa and P. E. Saikaly, *Chem. Mater.*, 2019, **31**, 3686.
6 N.-T. Suen, S.-F. Hung, Q. Quan, N. Zhang, Y.-J. Xu and H. M. Chen, *Chem. Soc. Rev.*, 2017, **46**, 337.
7 X. Cui, P. Ren, D. Deng, J. Deng and X. Bao, *Energy Environ. Sci.*, 2016, **9**, 123.
8 M. Wiechen, M. M. Najafpour, S. I. Allakhverdiev and L. Spiccia, *Energy Environ. Sci.*, 2014, **7**, 2203.
9 I. Roger, M. A. Shipman and M. D. Symes, *Nat. Rev. Chem.*, 2017, **1**, 1.
10 K. A. M. Ahmed, *J. Taibah Univ. Sci.*, 2016, **10**, 412.
11 T.-D. Dang, M. A. Cheney, S. Qian, S. W. Joo and B.-K. Min, *Ind. Eng. Chem. Res.*, 2013, **52**, 2750.
12 S. Kalathil and D. Pant, *RSC Adv.*, 2016, **6**, 30582.
13 B. E. Logan, R. Rossi, A. Ragab and P. E. Saikaly, *Nat. Rev. Microbiol.*, 2019, **17**, 307.
14 X. Fang, S. Kalathil, G. Divitini, Q. Wang and E. Reisner, *Proc. Natl. Acad. Sci. U. S. A.*, 2020, **117**, 5074.
15 A. Kumar, L. H-H. Hsu, P. Kavanagh, F. Barrière, P. N. L. Lens, L. Lapinsonnière, J. H. Lienhard, U. Schröder, X. Jiang and D. Leech, *Nat. Rev. Chem.*, 2017, **1**, 1.
16 M. Embree, Y. Qiu, W. Shieu, H. Nagarajan, R. O'Neil, D. Lovley and K. Zengler, *Appl. Environ. Microbiol.*, 2014, **80**, 2918.
17 M. Estevez-Canales, A. Kuzume, Z. Borjas, M. Füeg, D. Lovley, T. Wandlowski and A. Esteve-Núñez, *Environ. Microbiol. Rep.*, 2015, **7**, 219.
18 V. K. K. Praneeth, M. Kondo, M. Okamura, T. Akai, H. Izu and S. Masaoka, *Chem. Sci.*, 2019, **10**, 4628.
19 B. M. Hunter, N. B. Thompson, A. M. Müller, G. R. Rossman, M. G. Hill, J. R. Winkler and H. B. Gray, *Joule*, 2018, **2**, 747.
20 M. D. Yates, R. D. Cusick and B. E. Logan, *ACS Sustainable Chem. Eng.*, 2013, **1**, 1165.
21 K. S. Siddiqi, A. Husen and R. A. K. Rao, *J. Nanobiotechnol.*, 2018, **16**, 14.
22 A. H. Tanzil, S. T. Sultana, S. R. Saunders, A. C. Dohnalkova, L. Shi, E. Davenport, P. Ha and H. Beyenal, *Enzyme Microb. Technol.*, 2017, **95**, 69.
23 J. M. Byrne, H. Muhamadali, V. S. Coker, J. Cooper and J. R. Lloyd, *J. R. Soc., Interface*, 2015, **12**, 20150240.
24 A. Okamoto, Y. Tokunou, S. Kalathil and K. Hashimoto, *Angew. Chem., Int. Ed.*, 2017, **56**, 9082.

25 D. R. Bond and D. R. Lovley, *Appl. Environ. Microbiol.*, 2003, **69**, 1548.
26 J. R. Lloyd, C. Leang, A. L. Hodges Myerson, M. V. Coppi, S. Cuifo, M. Methe, S. J. Sandler and D. R. Lovley, *Biochem. J.*, 2003, **369**, 153.
27 T. S. Magnuson, N. Isoyoma, A. L. Hodges-Myerson, G. Davidson, M. J. Maroney, G. G. Geesey and D. R. Lovley, *Biochem. J.*, 2001, **359**, 147.
28 L. Laffont and P. Gibot, *Mater. Charact.*, 2010, **61**, 1268.
29 L. A. J. Garvie and A. J. Craven, *Am. Mineral.*, 1994, **79**, 411.
30 S. Zhang, K. J. T. Livi, A. C. Gaillot, A. T. Stone and D. R. Veblen, *Am. Mineral.*, 2010, **95**, 1741–1746.
31 S. K. Jana, B. Saha, B. Satpati and S. Banerjee, *Dalton Trans.*, 2015, **44**, 9158.
32 M. C. Biesinger, B. P. Payne, A. P. Grosvenor, L. W. M. Lau, A. R. Gerson and R. St. C. Smart, *Appl. Surf. Sci.*, 2011, **257**, 2717.
33 P. Kar, S. Sardar, S. Ghosh, M. R. Parida, B. Liu, O. F. Mohammed, P. Lemmens and S. K. Pal, *J. Mater. Chem. C*, 2015, **3**, 8200.
34 R. D. L. Smith, M. S. Prévot, R. D. Fagan, Z. Zhang, P. A. Sedach, M. K. J. Siu, S. Trudel and C. P. Berlinguette, *Science*, 2013, **340**, 60.
35 A. Yamaguchi, R. Inuzuka, T. Takashima, T. Hayashi, K. Hashimoto and R. Nakamura, *Nat. Commun.*, 2014, **5**, 4256.
36 J. Lai, S. Li, F. Wu, M. Saqib, R. Luque and G. Xu, *Energy Environ. Sci.*, 2016, **9**, 1210.
37 Y. Meng, W. Song, H. Huang, Z. Ren, S.-Y. Chen and S. L. Suib, *J. Am. Chem. Soc.*, 2014, **136**, 11452.
38 G. Mattioli, I. Zaharieva, H. Dau and L. Guidoni, *J. Am. Chem. Soc.*, 2015, **137**, 10254.
39 P. W. Menezes, A. Indra, P. Littlewood, M. Schwarze, C. GÖbel, R. Schomäcker and M. Driess, *ChemSusChem*, 2014, **7**, 2202.
40 C. C. L. McCrory, S. Jung, J. C. Peters and T. F. Jaramilo, *J. Am. Chem. Soc.*, 2013, **135**, 16977.
41 T. Takashima, K. Hashimoto and R. Nakamura, *J. Am. Chem. Soc.*, 2012, **134**, 1519.
42 L. Trotochaud, S. L. Young, J. K. Ranney and S. W. Boettcher, *J. Am. Chem. Soc.*, 2014, **136**, 6744.
43 J. Zhang and L. Dai, *Angew. Chem., Int. Ed.*, 2016, **55**, 13296.
44 R.-B. Song, Y. C. Wu, Z.-Q. Lin, J. Xie, C. H. Tan, J. S. C. Loo, B. Cao, J.-R. Zhang, J.-J. Zhu and Q. Zhang, *Angew. Chem., Int. Ed.*, 2017, **56**, 10516.
45 Y. Gorlin and T. F. Jaramillo, *J. Am. Chem. Soc.*, 2010, **132**, 13612.
46 H. Sim, J. Lee, T. Yu and B. Lim, *Korean J. Chem. Eng.*, 2018, **35**, 257.
47 H. Antoni, W. Xia, J. Masa, W. Schuhmann and M. Muhler, *Phys. Chem. Chem. Phys.*, 2017, **19**, 18434.
48 H. Antoni, D. M. Morales, Q. Fu, Y.-T. Chen, J. Masa, W. Schuhmann and M. Muhler, *ACS Omega*, 2018, **3**, 11216.
49 X. Zheng, L. Yu, B. Lan, G. Cheng, T. Lin, B. He, W. Ye, M. Sun and F. Ye, *J. Power Sources*, 2017, **362**, 332.
50 A. Mathur and A. Halder, *Catal. Sci. Technol.*, 2019, **9**, 1245.
51 G. Liu, J. Hall, N. Nasiri, T. Gengenbach, L. Spiccia, M. H. Cheah and A. Tricoli, *ChemSusChem*, 2015, **8**, 4162.
52 A. Ramírez, P. Hillebrand, D. Stellmach, M. M. May, P. Bogdanoff and S. Fiechter, *J. Phys. Chem. C*, 2014, **118**, 14073.
53 J. Guan, Z. Duan, F. Zhang, S. D. Kelly, R. Si, M. Dupuis, Q. Huang, J. Q. Chen, C. Tang and C. Li, *Nat. Catal.*, 2018, **1**, 870.
54 S. Lian, M. P. Browne, C. Domínguez, S. N. Stamatin, H. Nolan, G. S. Duesberg, M. E. G. Lyons, E. Fondab and P. E. Colavita, *Sustainable Energy Fuels*, 2017, **1**, 780.
55 K. R. Park, J. E. Jeon, G. Ali, Y.-H. Ko, J. Lee, H. S. Han and S. Mhin, *Catalysts*, 2019, **9**, 564.